Linear Weingarten membranes with funicular boundaries

Xavier Tellier, Cyril Douthe, Laurent Hauswirth, Olivier Baverel

Linear Weingarten membranes with funicular boundaries

Postprint – article published in Structural Concrete *of April 2020*

Xavier Tellier, PhD Candidate[1,2] *

Cyril Douthe, Researcher[1]

Laurent Hauswirth, Professor[2]

Olivier Baverel, Professor[1,3]

1 Laboratoire Navier (Ecole des Ponts, IFSTTAR, CNRS), Marne-la-Vallée, France
2 Université Paris-Est, Laboratoire d'Analyse et de Mathématiques Appliquées, Marne-la-Vallée, France
3 ENSA Grenoble, France
** Corresponding author: xavier.tellier@enpc.fr, +33 1 64 15 37 35, Laboratoire Navier, 77455 Champs-sur-Marne - MLV Cedex 2, FRANCE*

Abstract

Designing a curved architectural envelope is a challenging task, as it requires a balance between structural efficiency, fabricability and architectural requirements. In this article, we introduce a new conceptual design tool: Linear-Weingarten membranes, with boundaries either simply supported or realized as funicular cables or arches. We present a generation method for these surfaces, with a focus on how to treat free funicular boundaries. The method uses a surface discretization by triangular meshes, and computes a shape iteratively by a combination of dynamic relaxation and guided projections. The method can be used to generate the shape of self-stressed membranes, funicular vaults, and gridshells. For gridshells, the method allows to find geometries that combine mechanical performance and ease of fabrication.

Keywords:
Structural design, architectural geometry, Linear-Weingarten surfaces, membranes, funicular structures, static equilibrium, minimal surfaces, fabrication-aware design, planar quad meshes

1 Introduction

In the past decades, double curvature structural envelopes have become increasingly popular. Double curvature structures are attractive for several reasons. Firstly, their shape are expressive, and can give a unique character to a building. Secondly, curved shapes can be highly efficient mechanically. A remarkable example is the concrete shell of the CNIT (Paris), which spans 52m with a thickness of only 8cm (Figure 1).

Three types of structures are nowadays popular for constructing a double curvature envelope: tensile membranes, gridshells and funicular vaults. Historically, membranes were arguably the first non-dome type of double-curvature structure. The exploration of their formal potential was helped by the study of minimal surfaces. These surfaces, so named because they span a boundary with minimal area, correspond to the shape naturally taken by a soap film at equilibrium without external loading. An extensive experimental program was launched by Frei Otto's team (Bach, Burkhard, & Otto, 1988) to explore possible forms. In particular, this work led to the design of iconic structures such as the Olympic Stadium Munich (Figure 1).

Many recent research projects in structural engineering focus on how to reduce the environmental impact of buildings. One strong line of research in this respect is the study of funicular structures (see for example (Akbarzadeh, Van Mele, & Block, 2015; Block, 2009; Konstantatou, D'Acunto, & McRobie, 2018; Ohlbrock & Schwartz, 2016)). Funicular structures can resist one given load without bending, with pure axial forces. This makes them highly efficient. As a result, they allow to build a structure with a relatively low amount of materials. They can also be used to build with materials that have low or medium performance (Block, Davis, DeJong, & Ochsendorf, 2010), thus allowing to use more local or less polluting materials. One particular family of funicular surfaces are constant mean curvature (CMC) surfaces. These surfaces are funicular for a uniform pressure load, and correspond to the equilibrium shape of an inflated soap bubbles. Their formal potential for curved architectural envelopes was also demonstrated in (Bach et al., 1988). Applications to fabrication-aware design of gridshells were proposed in (Tellier, Hauswirth, Douthe, & Baverel, 2018).

Figure 1 Double curvature structural envelopes. Left: The concrete shell of the CNIT, Paris (©Alexandre Prevot). Right: Cable net of the Olympic Stadium, Münich

Minimal and CMC surfaces, despite being rich groups of surfaces, can sometimes offer a design space that is too limited for a given project. However, they belong to a much wider family of surfaces: the Linear-Weingarten (LW) surfaces, which are the topic of the present paper. This family of surfaces includes minimal surfaces and CMC, but also developable surfaces, pseudo-spheres, and a large array of surfaces in-between. A LW surface is characterized by the fact that, at any point, the mean and Gaussian curvature satisfy an affine relation, with constant coefficients throughout the surface:

$$aH + bK = c \quad / \quad a, b, c \in \mathbb{R} \tag{1}$$

These surfaces offer an interesting alternative to popular free-form design methods such as NURBS surfaces, as they offer both mechanical and geometrical properties. These properties will be detailed in section 2. Despite the wealth of knowledge gathered by the differential geometry community on LW surfaces, their application for design purposes have not been studied, mostly because no generation method was available. We introduced in (Tellier, Douthe, Baverel, & Hauswirth, n.d.) an algorithm to generate elliptical LW surfaces fitting closed boundary curves. However, two topics have not been addressed yet.

Firstly, the proposed method could just deal with fixed boundaries, and was therefore not able to model shells with openings bordered by funicular arches, or the geometry of membraned restrained by cables. This paper addresses this shortfall in section 3. Dynamic relaxation is used to find a funicular boundary compatible with the stress field of a LW surface. Secondly, the use of LW for structural design was not explored. Sections 4 investigates their potential for membrane, gridshell and funicular vault design. This paper is an extended version of the conference proceedings presented in (Tellier, Douthe, Hauswirth, & Baverel, 2019).

2 Properties of Linear Weingarten surfaces

2.1 Mechanical properties

(Rogers & Schief, 2003) showed an interesting link between LW surfaces and shell mechanics. LW surfaces correspond to equilibrium shapes of membranes under uniform pressure. Membranes are highly efficient mechanical structures: they are shell structures that can resist a given load with pure in-plane stresses, without bending stresses. Furthermore, for a LW membrane subject to uniform pressure of amplitude c, membrane stresses are known explicitly, and principal stresses are aligned with principal curvature directions:

$$\mathrm{N}_{11} = \mathrm{a} + \frac{\mathrm{b}}{2}\mathrm{k}_2 \;;\; \mathrm{N}_{12} = 0 \;;\; \mathrm{N}_{22} = \mathrm{a} + \frac{\mathrm{b}}{2}\mathrm{k}_1 \tag{2}$$

Where directions 1 and 2 are the principal curvature directions, k_1 and k_2 are the associated principal normal curvatures, and $\mathrm{N_{ij}}$ are the components of the membrane stress tensor **N**. These equations can be written in intrinsic form:

$$\mathbf{N} = a\mathbf{I} + \frac{b}{2}\hat{\mathbf{S}} \tag{3}$$

Where **I** is the identity of the tangent plane of the surface and $\hat{\mathbf{S}}$ is the curvature tensor (known as shape operator in surface theory), rotated by 90° in the tangent plane (in differential geometry notations: $\hat{\mathbf{S}} = \mathrm{J}\mathbf{S}$).

A particular case is obtained when $c = 0$: the LW surfaces then correspond to self-stressed membranes, like the ones showed in Figure 8. The fact that stresses are known analytically allows to give quick structural feedback to the designer, without having to transfer the geometry to an FE software.

2.2 Geometrical properties

Curvature lines of a surface can be used in many different ways to rationalize the fabrication of a double-curvature structure. In particular, they can be used to design gridshells covered with planar quadrangles and with nodes without geometrical torsion (Pottmann, Eigensatz, Vaxman, & Wallner, 2015). On an arbitrary surface, curvature lines tend to form an erratic network. For example, Figure 2 shows the curvature lines on the roof of the Visconti court in Le Louvres, designed by architects Ruddy Riciotti ad Mario Bellini. The configuration is badly suited for a gridshell: there is a high

variation in the size and aspect ratio of faces, beams have a poor mechanical alignment, and the pattern is subjectively unaesthetic - consequently, a triangular pattern was chosen. On LW surfaces, beyond the mechanical properties discussed in the previous section, curvature lines tend to form a fair network. This property is due to the fact they are offsets of constant mean curvature surfaces (Eisenhart, 1909). In particular, there cannot be singularities of index ½ like the ones highlighted with red dots in Figure 2 (Hartman & Wintner, 1954).

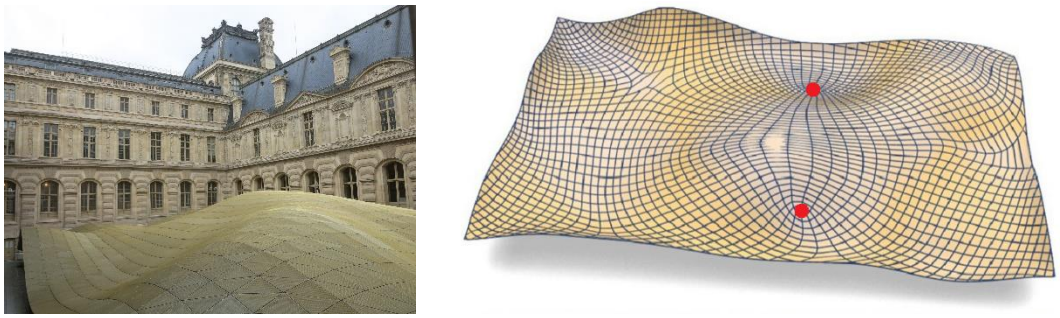

Figure 2 Curvature lines of the roof of the Visconti court in Le Louvre (reproduced with permission from (Wallner & Pottmann, 2011)*)*

A second important geometrical property is that equation (1) is a 2nd order partial differential equation on surface coordinates. Hopf (Hopf, 1983) showed that if $a^2 + bc > 0$, this equation is elliptic. This means that we can solve the following Dirichlet problem: generating a LW surface on a given closed boundary curve. This type of problem is often encountered when covering an existing atrium.

3 Generation

In this section, we propose a generation method of LW surfaces with cable boundaries. The resolution is iterative, and based on triangular meshes. Interior points and cable points are treated differently.

3.1 Interior points

In (Tellier et al., 2019), we proposed a first method to generate LW surfaces with fixed boundaries. We then introduced a more robust method in (Tellier 2020). This method relies on a discrete model of LW surfaces. Discrete LW surfaces are defined as the triangular meshes T which are the critical points of a linear combination E_1 of the area, total mean curvature, and volume:

$$\mathrm{E}_1(T) = \frac{\mathrm{a}}{2}\mathrm{Area}(T) + \mathrm{b}\mathrm{H}_{\mathrm{tot}}(T) + \mathrm{c}Vol(T) \tag{4}$$

Equivalently, these meshes verify at each vertex v:

$$\mathrm{a}\,\vec{\mathrm{H}}(\mathrm{v}) + \mathrm{b}\,\vec{\mathrm{K}}(\mathrm{v}) = \mathrm{c}\,\vec{\mathrm{n}} \tag{5}$$

where:

- $\vec{\mathrm{H}}(\mathrm{v}) = \frac{-3}{2\|\vec{A}(v)\|}\nabla_p \mathrm{Area}(\mathrm{T})$ is the mean curvature vector of vertex v ($\vec{A}(v)$ is the vector area of vector of the polyline joining the vertices adjacent to v);
- $\vec{\mathrm{K}}(\mathrm{v}) = \frac{-3}{2\|\vec{A}(v)\|}\sum_{\vec{e}\sim v}\theta_e \frac{\vec{e}}{\|\vec{e}\|}$ is the Gaussian curvature vector ot vertex v. The sum is taken over the edges $\vec{e}$ adjacent to v, and depends on the dihedral angle θ_e of each edge;
- $\vec{\mathrm{n}}$ is the normal vector at v, defined as a unit vector aligned with the vector area $\vec{A}(v)$.

A simple gradient descent is not robust to generate LW surfaces, as functional E_1 is not convex. In (Tellier 2020), we proposed an algorithm based on iterative projections. It uses the partition of elliptical LW surfaces in two families, called type I and type II. We will use this method for interior points (i.e. points not located on the mesh boundary) in this article.

3.2 Cable boundary

Tensile membranes are usually held at their boundaries by cables. In this section, we investigate how this can be modelled with LW surfaces, and how to generate the shape of LW surfaces bordered by cables. This question is also of interest for the design of funicular shells with openings, for which openings are realized with funicular arches.

This problem can be understood as a generalization of the Euler-Plateau problem introduced in (Giomi & Mahadevan, 2012). This problem considers minimal surfaces for which the boundary is an elastica, i.e. a curve of imposed length minimizing the integral of its squared curvature. (Pérez, Otaduy, & Thomaszewski, 2017) generalized this problem to Kirchoff rods, which are minimizers of a sum of a curvature and a torsional energy. Our problem is a generalization of the one of Giomi in a sense that we do not consider minimal, but LW surfaces. We are however interested only in boundaries curves without bending energy, as we aim at obtaining funicular shapes.

This section is divided in four parts. First, we derive the geometrical equations verified by the boundary, and how the cable tension varies. Based on the equilibrium equations, we propose a discrete model of the boundary. We then introduce a generation method using dynamic relaxation. Finally, the generation method is validated on a test case.

3.2.1 Equilibrium and geometry

One convenient method to generate LW surfaces bordered by cables would be to minimize an energy composed of the sum of an energy associated with the LW surface and the elastic energy of the cable: $E = E_{LW} + E_{cable}$. However, the variational formulations of LW surfaces in the literature address only surfaces without boundaries. We therefore use an equilibrium approach to treat the boundary.

Equilibrium of a membrane cable

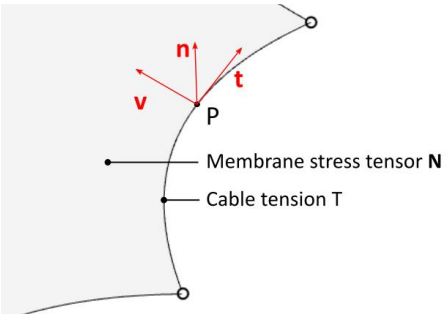

Figure 3 Equilibrium of a boundary cable

Let us consider a cable parametrized by arc length s with an associated Darboux frame $(\mathbf{t}, \mathbf{v}, \mathbf{n})$, where $\mathbf{t}$ is the tangent vector to the cable, $\mathbf{n}$ is the surface normal, and $\mathbf{v}$ is a unit vector in the tangent plane orthogonal to the boundary (Figure 3). The cable has an a tension T and is subjected only to membrane stresses (with stress tensor $\mathbf{N}$), other forces are supposed to be negligible. The equilibrium of the cable can then be written:

$$\frac{\mathrm{d}}{\mathrm{ds}}(\mathrm{T}\mathbf{t}) + \mathbf{N}.\mathbf{v} = 0$$

This can be developed into:

$$\frac{\mathrm{dT}}{\mathrm{ds}}\mathbf{t} + \mathrm{T}\frac{\mathrm{d}\mathbf{t}}{\mathrm{ds}} + \mathrm{N_{vv}}\mathbf{v} + \mathrm{N_{tv}}\mathbf{t} = 0$$

We can express the derivative of the tangent vector $\mathbf{t}$ using the derivatives of the vectors of the Darboux frame:

$$\frac{\mathrm{d}\mathbf{t}}{\mathrm{ds}} = \mathrm{k_g}\mathbf{v} + \mathrm{k_n}\mathbf{n}$$

Projecting the equilibrium equation along $\mathbf{v}$, $\mathbf{t}$ and $\mathbf{n}$, we obtain successively:

$$\mathrm{T}\,\mathrm{k_g} + \mathrm{N_{vv}} = 0 \tag{6}$$

$$\frac{\mathrm{dT}}{\mathrm{ds}} = -\mathrm{N_{tv}} \tag{7}$$

$$\mathrm{k_n} = 0 \tag{8}$$

We note that, in the case of a sliding cable, $N_{tv} = 0$, so $\frac{dT}{ds} = 0$: the tension in the cable is constant.

LW membrane stresses at boundary

Let us now express the LW membrane stresses at the boundary. We recall that the corresponding membrane stress tensor is:

$$\mathbf{N} = \mathrm{a}\,\mathbf{I} + \frac{\mathrm{b}}{2}\,\hat{\mathbf{S}}$$

For a unit vector $\mathbf{v}$ of the tangent plane perpendicular to the boundary:

$$\mathbf{N}.\mathbf{v} = \mathrm{a}\,\mathbf{v} + \frac{\mathrm{b}}{2}\hat{\mathbf{S}}.\mathbf{v}$$

In order to obtain the component N_{vv} of the membrane stress tensor, we express $\mathbf{v}$ in the basis of principal curvature directions: $\mathbf{v} = \cos\theta\,\boldsymbol{e_1} + \sin\theta\,\boldsymbol{e_2}$ where $\boldsymbol{e_1}$ and $\boldsymbol{e_2}$ are unit vectors aligned with principal directions. The vector $\mathbf{t}$ can be expressed in that same basis: $\mathbf{t} = \cos\left(\theta - \frac{\pi}{2}\right)\boldsymbol{e_1} + \sin\left(\theta - \frac{\pi}{2}\right)\boldsymbol{e_2}$. We obtain:

$$\mathbf{v}.\mathbf{N}.\mathbf{v} = \mathrm{a} + \frac{\mathrm{b}}{2}(\cos\theta \;\; \sin\theta)\begin{bmatrix}\mathrm{k_2} & 0\\ 0 & \mathrm{k_1}\end{bmatrix}\begin{pmatrix}\cos\theta\\ \sin\theta\end{pmatrix} = \mathrm{a} + \frac{\mathrm{b}}{2}(\mathrm{k_2}\cos^2\theta + \mathrm{k_1}\sin^2\theta)$$

$$= \mathrm{a} + \frac{\mathrm{b}}{2}\left(\mathrm{k_2}\sin^2\left(\theta - \frac{\pi}{2}\right) + \mathrm{k_1}\cos^2\left(\theta - \frac{\pi}{2}\right)\right)$$

$$N_{vv} = a + \frac{b}{2}k_n \tag{9}$$

where k_n is the normal curvature of the boundary. We observe that the normal membrane stress component due to the term bK in $aH + bK = c$ is proportional to the normal curvature of the boundary, which vanishes at equilibrium.
The shear component is:

$$\mathbf{t}.\mathbf{N}.\mathbf{v} = \mathrm{a} + \frac{\mathrm{b}}{2}(\sin\theta \ \ -\cos\theta)\begin{bmatrix}\mathrm{k}_2 & 0\\ 0 & \mathrm{k}_1\end{bmatrix}\begin{pmatrix}\cos\theta\\ \sin\theta\end{pmatrix} = \frac{\mathrm{b}}{2}(\mathrm{k}_2 - \mathrm{k}_1)\cos\theta\sin\theta$$

$$\mathrm{N}_{\mathrm{tv}} = \frac{\mathrm{b}}{2}\tau_{\mathrm{g}} \tag{10}$$

where τ_g is the geodesic torsion of the boundary (see (do Carmo, 1976) for the derivation of $\tau_g = (k_2 - k_1)\cos\theta\sin\theta$).

Geometry of a cable attached to a LW membrane

By combining the equilibrium equations of the cables with the LW stresses, we find that the geometry of the boundary must fulfil two geometrical differential equations.
The first one was already derived from the equilibrium of the cable (equation 8):

$$\boxed{k_n = 0} \tag{8}$$

It implies that the cable follows an asymptotic line on the surface. For the second one, we first observe using equation (*9*) that the normal stress at the boundary is $N_{vv} = a$. Equation (6) implies:

$$k_g = \frac{a}{T}$$

This equation can be combined with the equation *7* to remove variable T. It has different geometrical implications depending on whether b is null or not.

- **If $\boldsymbol{b = 0}$** (i.e. the surface is CMC), we obtain from equation (*10*) that the shear is null:

  $$N_{tv} = 0$$

  Consequently, equation (6) yields:

  $$\frac{dT}{ds} = 0$$

As a result:

$$\boxed{\frac{dk_g}{ds} = 0} \tag{12}$$

This means that the geodesic curvature of the boundary is constant. Not all CMC surfaces admit an asymptotic line with constant geodesic curvature. For example, one can find such lines on a helicoid, but not on a catenoid. The presence of a boundary cable has therefore a strong impact on the surface geometry.

- **If $\boldsymbol{b \neq 0}$**, we have to consider separately the case of a sliding cable and the case of a cable attached to the membrane:
  - Sliding cable: $N_{tv} = 0$ implies that :

$$\boxed{\tau_g = 0} \tag{13}$$

$\tau_g = 0$ means that the cable follows a curvature line. Since both the normal curvature and the torsion of the boundary are null, it is necessarily planar.

  - Fixed cable:

$$\frac{\mathrm{b}}{2}\tau_{\mathrm{g}} = -\mathrm{N}_{\mathrm{tv}} = -\frac{\mathrm{dT}}{\mathrm{ds}} = -\mathrm{a}\frac{\mathrm{d}}{\mathrm{ds}}\left(\frac{1}{\mathrm{k}_{\mathrm{g}}}\right)$$

$$\boxed{\frac{b}{2}\tau_g = \frac{a}{k_g^2}\frac{dk_g}{ds}} \tag{14}$$

Similarly to the case $b = 0$, the quantity $\frac{\mathrm{k}_{\mathrm{g}}'}{\tau_{\mathrm{g}}\,\mathrm{k}_{\mathrm{g}}^2}$ is not constant for an arbitrary asymptotic line of an arbitrary LW surface.

3.2.2 Discrete model

We propose to discretize boundary cables as series of particles connected by springs. This section describes the discrete model of forces acting on particles for a non-sliding cable. Each particle is subject to a tension from the cable and to membrane stresses (Figure 4). Cable forces are computed from the elastic elongation of the cable:

$$\boldsymbol{f_{cable}} = k\left(l_1 - l_{1,i}\right)\boldsymbol{u_1} + k\left(l_2 - l_{2,i}\right)\boldsymbol{u_2}$$

Where:

- $\mathbf{u_i}$ is the unit vector from P to P_i: $\mathbf{u_1} = \frac{\overrightarrow{\mathrm{PP_1}}}{\|\overrightarrow{\mathrm{PP_1}}\|}$; $\mathbf{u_2} = \frac{\overrightarrow{\mathrm{PP_2}}}{\|\overrightarrow{\mathrm{PP_2}}\|}$
- l_1 and $l_{1,i}$ are respectively the current and the initial length of line PP_1.

Membrane forces are computed by integrated the stresses calculated in the previous section over a portion of cable of length $\frac{\|\overrightarrow{PP_1}\|+\|\overrightarrow{PP_2}\|}{2}$ centered at P:

$$\boldsymbol{f_{membrane}} = -a\,\nabla_{\mathrm{p}}\mathrm{A} - \frac{b}{2}T_g\,\boldsymbol{t}$$

Where:

- $\nabla_{\mathrm{p}}\mathrm{A}$ is the gradient of the summed areas of the mesh triangles adjacent to P. This term corresponds to the normal component of membrane stresses $N_{vv} = a$ (equation 6.9) integrated over the length of the portion of cable. We ignore the term $\frac{b}{2}k_n(\boldsymbol{t})$ of equation 6.9, because it vanishes at convergence anyway.
- **t** is the tangent vector of the boundary curve, computed as :

$$\mathbf{t} = \frac{\mathrm{P_2} - \mathrm{P_1}}{\|\mathrm{P_2P_1}\|}$$

- T_g is the halved torsion angle from the normal at P2 to the normal at P1, computed as:

$$T_g = \frac{1}{2}\arcsin\left(\det\left(\mathbf{n_1^p}, \mathbf{n_2^p}, \mathbf{t}\right)\right)$$

Where $\mathbf{n_i^p}$ is the projection of the normal vector $\mathbf{n_i}$ at Pi onto the plane (P,t,n). The normal vector **n** is simply computed as the normal of the plane (PP_1P_2). To model a sliding cable, one just needs to write the membrane force as $\boldsymbol{f_{membrane}} = -a\,\nabla_{\mathrm{p}}\mathrm{A}$.

Note 1: This way of computing the normal requires to special treatment if boundary points are aligned (or nearly aligned). A more robust scheme would be to approximate locally the surface by a paraboloid.

Note 2: The calculation of the torsion requires a consistent orientation of the boundary curve. This orientation is determined by the orientation of the tangent vector **t**.

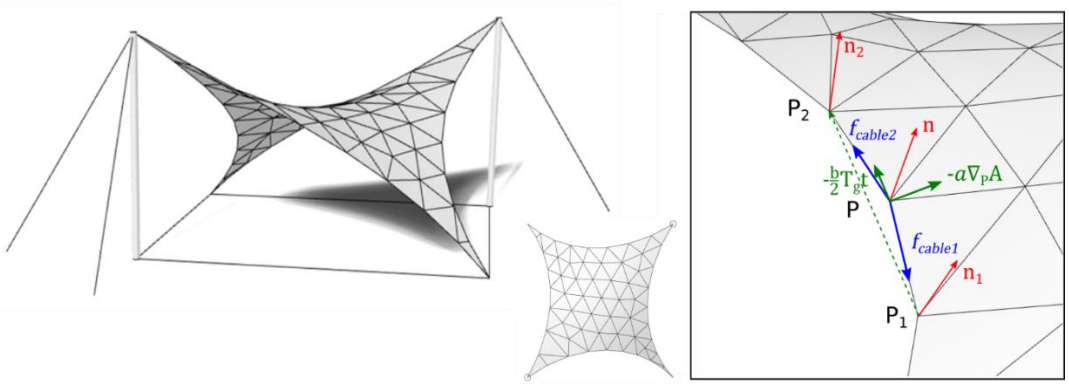

Figure 4 Equilibrium of vertex of a boundary cable

3.2.3 Dynamic relaxation

We look for the equilibrium position of the boundary cables with a dynamic relaxation approach (Otter, Cassel, & Hobbs, 1966). This procedure is done simultaneously with the projection approach for the non-boundary points, as will be explained in section 3.3.

The motion of a particle P of a cable is given by:

$$m\ddot{P} = \boldsymbol{f_{cable}} + \boldsymbol{f_{membrane}}$$

This equation can for example be discretized as (Douthe, 2007):

$$P_{i,t} = P_{i,t-1} + \dot{P}_{i,t-1}\Delta t + \frac{\Delta t^2}{m_i}\left(\boldsymbol{f_{cable}} + \boldsymbol{f_{membrane}}\right)$$

The interior points are computed by projections at each iteration (as explained in section 3.1), so they do not conserve their momentum. In order to have a consistent model for both boundary and interior points, we ignore particle momentum at the boundaries by setting $\dot{P}_{i,t-1} = 0$. This is equivalent to applying a so-called kinematic damping at each step. Our numerical scheme therefore reads:

$$P_{i,t} = P_{i,t-1} + \frac{\Delta t^2}{m_i}\left(\boldsymbol{f_{cable}} + \boldsymbol{f_{membrane}}\right)$$

We use $\Delta t = 1$ and a mass proportional to the length of cable, with constant lineic mass:

$$m_i = \rho\,\frac{\|\overrightarrow{PP_1}\| + \|\overrightarrow{PP_2}\|}{2}$$

Where ρ is adjusted manually to obtain proper speed while avoiding oscillations (which appear near equilibrium if a value too low is chosen).

We iterate until a position is found where $\|\boldsymbol{f}_{cable} + \boldsymbol{f}_{membrane}\| < \boldsymbol{\varepsilon}$. This algorithm converged in all the tested cases. Once convergence is reached, equilibrium is guaranteed.

Mode advanced numerical schemes could be developed to deal with boundary and interior points in a more uniform approach. This could be achieved by deriving a variational formulation of the cable-boundary problem.

3.2.4 Validation

Once the algorithm has converged, the geometry of boundaries can be validated by checking that the two differential equations (*8*) and (*14*) are verified.

$k_n = 0$ is automatically verified at equilibrium: since $\boldsymbol{t}$,$\boldsymbol{u_1}$ and $\boldsymbol{u_2}$ are always coplanar, the membrane force $\nabla_p A$ belongs to that plane at equilibrium. The tangent plane of the membrane, oriented by $\boldsymbol{t}$ and $\nabla_p A$, contains then the circle fitting PP_1P_2: the curvature of the cable is purely geodesic, so the normal curvautre is null.

Equation (*14*) can be validated by calculating the geodesic curvature at each point. We evaluate it by taking the inverse of the radius of the circle fitting PP_1P_2. We then use a finite difference scheme to evaluate the derivative:

$$\frac{\mathrm{dk_g}}{\mathrm{ds}} = \frac{\mathrm{k_g(P_2)} - \mathrm{k_g(P_1)}}{\mathrm{l_1} + \mathrm{l_2}}$$

Figure 5 shows how equation (*14*) is verified for a LW surface bordered by cables anchored at four points. The ratio $\frac{b}{2}\tau_g / a\frac{k'_g}{k_g^2}$ is theoretically 1. In practice, its value is not exactly 1, but remains between 0.9 and 1.1, except at cable extremities (blue dots) and at one point near the middle of the cables (red dots) for which the numerator and denominator are near zero. The fact that the value is not exactly 1 can be mostly explained by the fact that torsion and geodesic curvature are calculated by different discrete models. Therefore, the generation method yields a cable position at equilibrium with the membrane tension, with a precision that is sufficient for our purpose.

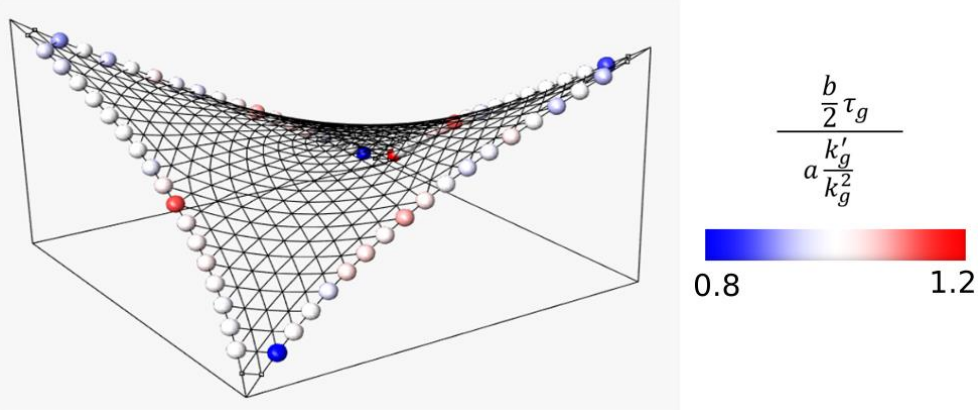

Figure 5 LW Verification of the geometry of boundary cables

3.3 Global resolution

The projection algorithm for interior points and the dynamic relaxation are used simultaneously in an interactive manner to deform a mesh towards a LW shape with valid cable boundaries. A user has four parameters at hand: the LW parameters a, b and c, and the cable stiffness k. The global resolution is summarized in Figure 6. Iterations are stopped if vertex displacements are below a certain value.

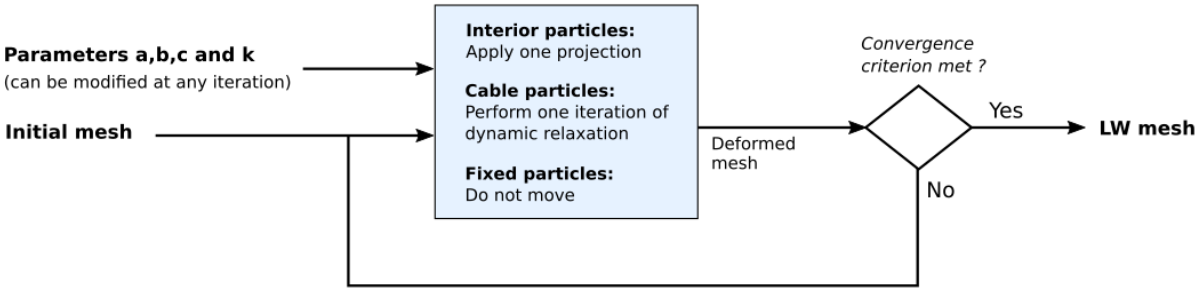

Figure 6 Combined resolution of interior points, cables and fixed points.

This iterative algorithms was implemented by scripting the software Rhino/Grasshopper. All the numerical images of this section were generated from that script. During this iteration process, the initial mesh might undergo large deformations. To avoid ending up with highly anisotropic faces, a remeshing tool was implemented. It performs an edge

flipping (see for example (Botsch, Kobbelt, Pauly, Alliez, & Lévy, 2010)) when a vertex is found inside the circumscribed of a neighbour triangle (more precisely, if the projection of the vertex is in the circle). Remeshing is manually triggered by the user.

4 Design applications

4.1 Tensile membranes

Tensile membranes allow to cover wide spans with a very low weight and limited cost. Formerly reserved for temporary structures such as circus tents, the recent technical advances in materials make it possible to ensure their durability for up to several decades.

4.1.1 Existing form finding methods

Tensile membranes have no out-of-plane stiffness, and their weight is negligible compared to external loads. Therefore, their shape is entirely determined by the geometry of their boundary and the distribution of the prestressing (plus the tension in valley cables if some are included). The geometrical design of a tensile membrane therefore amounts to determining these parameters. There are two main families of methods for this purpose.

The first is to build a minimal surface on the desired boundaries. Minimal surfaces can easily be created with wire and soap. There are also many easy-to-use algorithms for generating a minimal surface. These algorithms are based on the minimization of the area of a mesh. The resulting shapes correspond to membranes in which the prestress is isotropic and uniform. These surfaces are mechanically efficient, but offer a very limited design freedom.

The second is to prescribe pretension stresses using methods such as force densities (Schek, 1974), finite elements, or the updated reference strategy (Bletzinger, Wüchner, Daoud, & Camprubí, 2005). These methods allow to explore all the possible self-stressed forms on a given boundary, but require more work from the designer: The orientation of the principal stresses must be defined, trials and errors must be made on the values and directions of the pretension.

4.1.2 Linear Weingarten membranes

As discussed in section 2, LW surfaces with $c=0$ correspond to equilibrium shapes of self-stressed membranes. Therefore, our generation method can offer a new way of finding forms. With $a=1$, these surfaces verify:

$$H + bK = 0 \tag{7}$$

A designer therefore has one degree of freedom (the parameter b) to design a surface WL on a given edge; unlike with minimal surfaces, which are entirely determined by their boundary. Equation 2 shows that the parameter b modifies the prestressing ratio between the two main directions of curvature. Figure 7 and Figure 8show the effect of parameter b on the shape of a membrane on a fixed boundary. When $b \to \pm\infty$, the surface tends towards a developable surface (depending on the boundary, the surface might need to split in several portions to become developable).

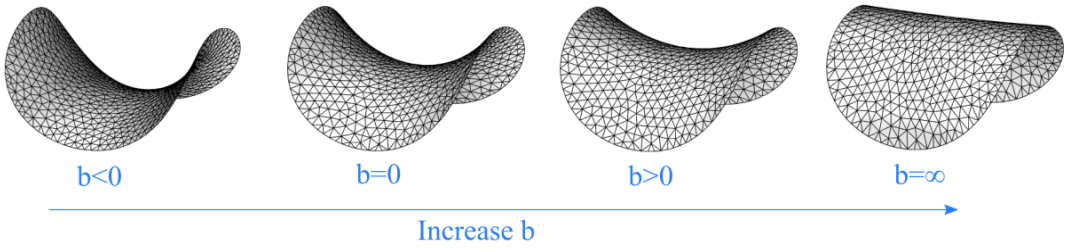

Figure 7 LW meshes generated on the same boundary with different values of parameter b

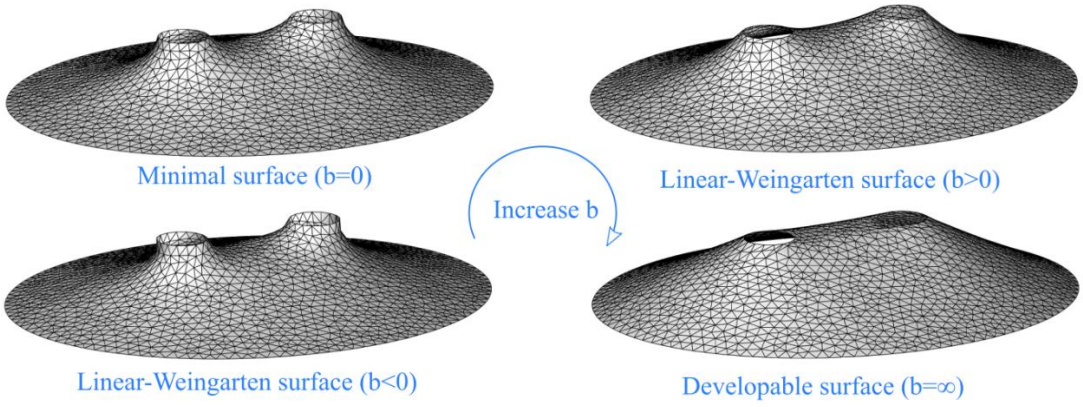

Figure 8 Series of "big top" membranes generated on the same boundary with different values of b

Our generation method is therefore a form-finding tool which is intermediate (in terms of design freedom and required labour) between minimal surfaces and the more advanced methods discussed in section 4.1.

4.1.3 Choice of parameter b

The parameter b affects the following aspects, which are often critical for the design of a tense membrane.

Height of canvas

By adjusting the value of *b*, one can change the average height of the surface. This effect is shown in Figure 10, where a minimal surface and a LW surface are built on the same two contours.

Water ponding

Tensile membranes must have a minimum slope in order to prevent the formation of water ponds. Parameter *b* also allows to modify this maximum slope, as shown in Figure 10.

Expressivity

Minimal surfaces tend to be relatively flat over large portions, this effect can be seen in Figure 9. By modifying parameter b, one can control the prestressing ratios (as shown in Figure 10), and curve these flat areas.

Stability

The Gaussian curvature of a surface characterizes its non-flatness. If too low, the surface is too flat, and may oscillate or even beat with the wind. Parameter *b* allows to modify the distribution of the Gaussian curvature to avoid this problem, as shown in Figure 10.

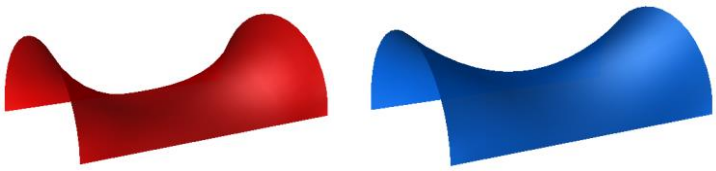

Figure 9 Left: Minimal surface. Right: LW surface on the same boundary.

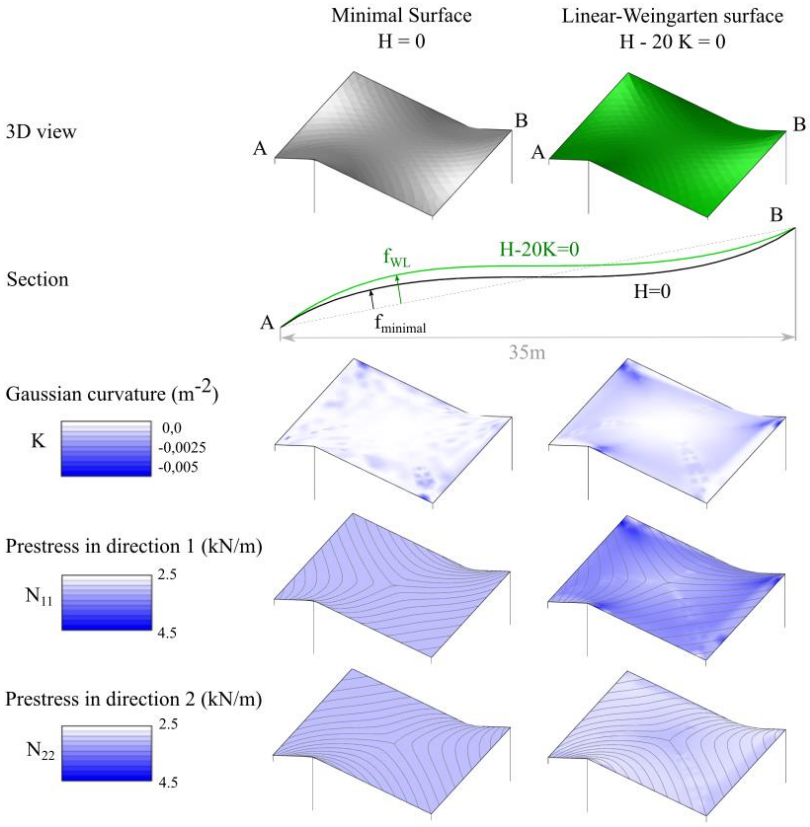

Figure 10 Comparison of the geometry and prestressing of a minimal and a LW membrane

4.1.4 Membranes attached by cables

Figure 11 shows examples of LW membranes ($c = 0$) bordered by non-sliding cables, shown in red. Anchor points of cables are shown with black dots. The left image shows a membrane bordered by a cable anchored at six points – lighting of mesh faces is voluntarily not smoothed to highlight the mesh geometry. The right image shows a LW surface with a hole bordered by a cable anchored at only one point.

Coming back to the LW surface of Figure 4, we observe in the top view that boundary cables are not circular. Geodesic curvature is higher near the low points. This is expected as the tension is higher in the direction of the diagonal between the high points.

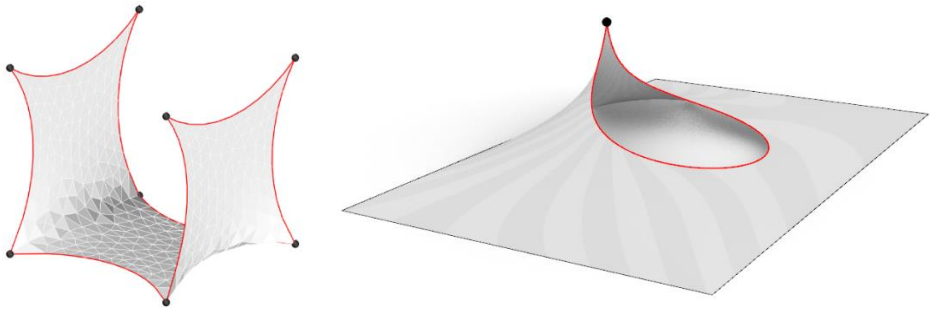

Figure 11 Examples of LW membranes bordered by cables

4.2 Gridshells

Gridshells are shells composed of a network of beams. In order to simplify the fabrication of such structures, it is often desirable to align the beams with principal curvature directions of the underlying surface (Pottmann et al., 2007): the surface can then be cladded by planar glass panels, only four beams meet at the nodes (unlike triangular meshes with complex 6-valent nodes), and the nodes are torsion-free, i.e. the median planes of the beams meet on a common axis. This property, illustrated in Figure 12, simplifies significantly the fabrication of the nodes, which are the costliest elements of this type of structure.

As discussed in section 2, curvature lines on LW surfaces have two properties. Firstly, they form a regular pattern, and secondly they are aligned with principal stresses under uniform pressure loading (assuming membrane-compatible supports are provided). When beams are not aligned with principal stresses, the grid is subjected to shear forces. Contrary to triangular lattices, quadrangular ones have a shear mechanism. Strength and rigidity in shear is usually obtained by one of these two means: adding diagonals (e.g. cables) or having clamped beam-beam connections. The second option is usually cheaper and preferred by architects, because cables tend to obstruct the view. However, it is impractical if shear forces are too high. In LW gridshells, the shear is null for one major load case: uniform wind load. LW gridshells are therefore good candidates to design cable-free gridshells. Future case studies will be performed to assess the variation of the orientation of the principal stresses under asymmetrical loads.

Figure 12 shows how a LW gridshell can be used to design an alternative structure for the glass roof of the British Museum in London, whose geometry is based on a triangular mesh. A surface surprisingly close to the real one can be obtained with a LW surface. The beam orientation is obtained by remeshing the LW triangular mesh following principal curvature directions.

Canopy of the great court of the British Museum.
The steel gridshell follows a triangular mesh.

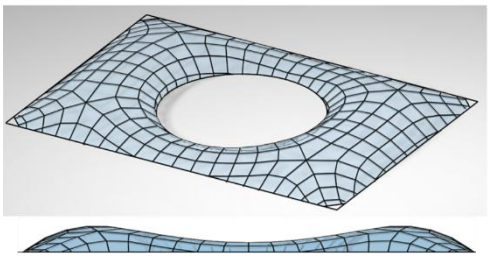

Linear-Weingarten surface on the same boundary,
with beams aligned with principal curvature directions.

Node with torsion

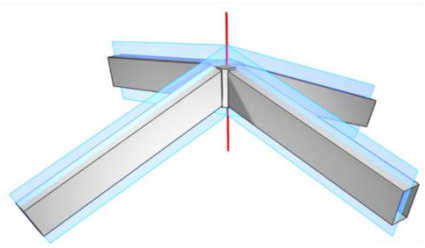

Torsion-free node

Figure 12 Proposition of an alternative geometry for the glass roof of the British Museum. The proposed geometry has flat panels, torsion-free nodes, and perfect mechanical beam orientation under uniform wind load. (bottom left picture: Romain Mesnil).

Figure 13 highlights the role of parameter *b* in the form of a gridshell. The geometry of the boundary of the Chadstone gridshell is replicated (height variations of the boundary are neglected). The upper figure shows a constant mean curvature surface (*b=0*) generated on this boundary. Heights are indicated at key points. The shape looks remarkably close to the one of the real gridshell. When *b* is increased, we observe that the height difference between hill tops and saddle points decreases: the crest line becomes more level. The opposite behaviour is observed when decreasing *b*: the higher variation of height makes the surface more expressive.

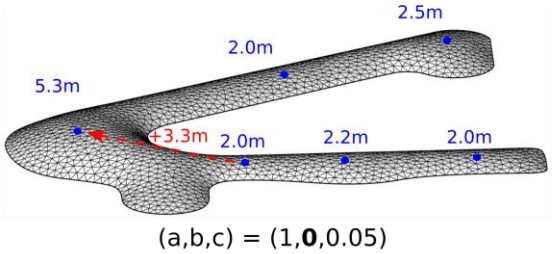

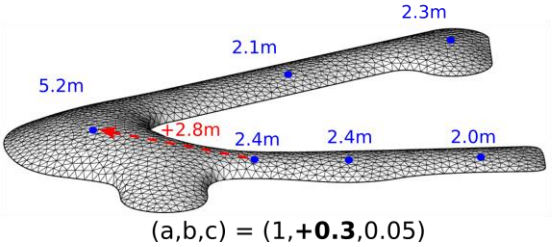

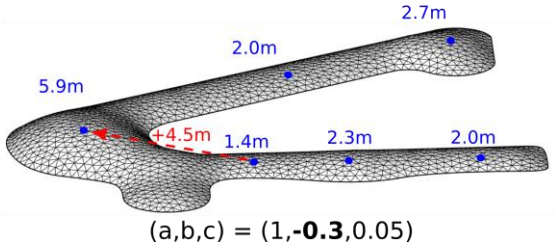

Figure 13 Linear-Weingarten surfaces generated on a boundary similar to the one of the Chadstone gridshell. Heights with respect to the plane containing the boundary line are indicated in blue. (Picture © Seele). Compared to the case b=0 (CMC surface), increasing b levels out the height, while decreasing b increases the height difference between saddle points and hill tops.

4.3 Funicular vaults

Figure 14 shows two LW vaults which are funicular in tension under a uniform upwards pressure load. The top image shows a CMC surface constructed on a circular boundary. Only a portion of the boundary is modelled as a cable. The resulting surface is not spherical, and is somehow shaped like a water droplet. When subjected to a downwards pressure load, the cable becomes a compression funicular polygon, which can be materialized by an arch with very low bending and tension resistance – such as a masonry arch.

The surface at the bottom is bordered by cables which are anchored at six points. Forces are transmitted only to the corners – this is often a constraint for covering of existing atriums. Interestingly, a small dome emerges at the angle of the L.

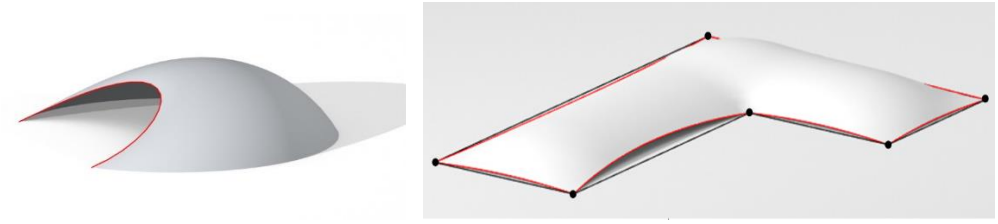

Figure 14 Examples of LW surfaces bordered by funicular arches

4.4 Single curvature panels

The method can be used to generate developable surfaces. This type of surface is useful to clad an envelope with thin flexible panels such as single layer tempered glass or metal sheets. Developable surfaces are a special type of Linear-Weingarten surfaces: they verify $a = c = 0$. For a given boundary, depending on the sign of b, two surfaces can be obtained by the algorithm. Together, they form the convex envelope of the curves. Therefore, the method is restricted to convex developable surfaces. This is discussed more in details in (Tellier et al., n.d.). An example is shown in Figure 15. A curve is drawn on a sphere, it delimits two portions of spheres, the upper one is triangulated. The right picture shows the result of the optimization (mesh edges are not displayed). The final shape is composed of portions of planes, portions of cylinders, and portions of general developable surfaces.

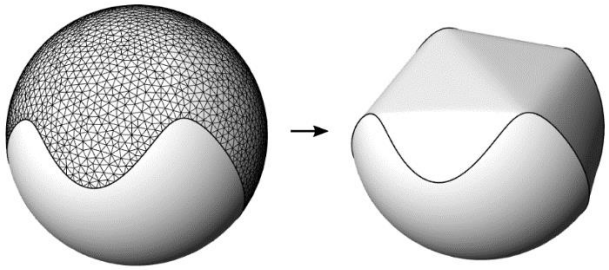

Figure 15 Developable surface generated from a curve on a sphere

5 Conclusion

In this paper, we presented how Linear Weingarten surfaces can be used as a design tool for double curvature structures. These surfaces, previously confined to the field of mathematics, have interesting mechanical, manufacturing, and aesthetic properties. We proposed a method to generate LW surfaces with both fixed and funicular boundaries. The method combines a projection method of the interior points with a dynamic relaxation for the cable points. Compared to other form-finding methods, Linear Weingarten membranes offer an interesting design freedom with a relatively low preprocessing work required from a designer. It is therefore well suited for a conceptual design tool. This study also allowed to advance the understanding of funicular membrane shapes. We showed how Linear Weingarten can be used to design self-stressed membranes, gridshells, and funicular vaults.

Acknowledgements

This work is supported by Labex MMCD (http://mmcd.univ-paris-est.fr/). The authors would like to thank Johannes Wallner for his help on discrete geometrical models.

References

Akbarzadeh, M., Van Mele, T., & Block, P. (2015). On the equilibrium of funicular polyhedral frames and convex polyhedral force diagrams. *CAD Computer Aided Design*, *63*, 118–128. https://doi.org/10.1016/j.cad.2015.01.006

Bach, K., Burkhard, B., & Otto, F. (1988). *IL18 Forming Bubbles*. Institute for Lightweight structures, University of Stuttgart.

Bletzinger, K. U., Wüchner, R., Daoud, F., & Camprubí, N. (2005). Computational methods for form finding and optimization of shells and membranes. *Computer Methods in Applied Mechanics and Engineering*, *194*(30-33

SPEC. ISS.), 3438–3452. https://doi.org/10.1016/j.cma.2004.12.026
Block, P. (2009). *Thrust Network Analysis. Exploring Three-dimensional Equilibrium*. MIT.
Block, P., Davis, L., DeJong, M., & Ochsendorf, J. (2010). Tile vaulted systems for low-cost construction in Africa. *African Technology Development Forum*, *7*(1), 4–13.
Botsch, M., Kobbelt, L., Paully, M., Alliez, P., & Lévy, B. (2010). *Polygon mesh processing*. AK Peters/CRC Press.
do Carmo, M. P. (1976). *Differential geometry of curves and surfaces*. Prentice-Hall, Inc.
Douthe, C. (2007). *Etude de structures élancées précontraintes en matériaux composites , application à la conception des gridshells*. Ecole des Ponts ParisTech.
Eisenhart, L. P. (1909). *A treatise on the differential geometry of curves and surfaces*. Ginn and Company Proprietors, Boston USA.
Giomi, L., & Mahadevan, L. (2012). Minimal surfaces bounded by elastic lines. *Proceedings of the Royal Society A: Mathematical, Physical and Engineering Sciences*, *468*(2143), 1851–1864. https://doi.org/10.1098/rspa.2011.0627
Hartman, P., & Wintner, A. (1954). Umbilical Points and W-Surfaces. *American Journal of Mathematics*, *76*(3), 502–508. Retrieved from https://www.jstor.org/stable/2372698
Hopf, H. (1983). *Differential Geometry in the Large, Lecture Notes in Math.* (BerlinHeidelberg-New York, Ed.).
Konstantatou, M., D'Acunto, P., & McRobie, A. (2018). Polarities in structural analysis and design: n-dimensional graphic statics and structural transformations. *International Journal of Solids and Structures*, *152–153*(July), 272–293. https://doi.org/10.1016/j.ijsolstr.2018.07.003
Ohlbrock, P. O., & Schwartz, J. (2016). Combinatorial equilibrium modeling. *International Journal of Space Structures*, *31*(2–4), 177–189. https://doi.org/10.1177/0266351116660799
Otter, J., Cassel, A., & Hobbs, R. (1966). Dynamic relaxation. In *Proceedings of the Institution of Civil Engineers* (pp. 633–656).
Pérez, J., Otaduy, M. A., & Thomaszewski, B. (2017). Computational design and automated fabrication of Kirchhof-Plateau surfaces. *ACM Transactions on Graphics*, *36*(4). https://doi.org/10.1145/3072959.3073695
Pottmann, H., Eigensatz, M., Vaxman, A., & Wallner, J. (2015). Architectural geometry. *Computers and Graphics (Pergamon)*, *47*, 145–164. https://doi.org/10.1016/j.cag.2014.11.002
Rogers, C., & Schief, W. K. (2003). On the equilibrium of shell membranes under normal loading. Hidden integrability. *Proceedings of the Royal Society A: Mathematical, Physical and Engineering Sciences*, *459*, 2449–2462. https://doi.org/10.1098/rspa.2003.1135
Schek, H. J. (1974). The force density method for form finding and computation of general networks. *Computer Methods in Applied Mechanics and Engineering*, *3*(1), 115–134. https://doi.org/10.1016/0045-7825(74)90045-0
Tellier, X.. (2020). Morphogenesis of curved structural envelopes under fabrication constraints [PhD Thesis]. Université Paris-Est; 2020
Tellier, X., Douthe, C., Hauswirth, L., & Baverel, O. (2019). Linear Weingarten surfaces for conceptual design. *Proceedings of the International Fib Symposium on Conceptual Design of Structures*, 225–232.
Tellier, X., Hauswirth, L., Douthe, C., & Baverel, O. (2018). Discrete CMC surfaces for doubly-curved building envelopes. In *Advances in Architectural Geometry* (pp. 166–193).
Wallner, J., & Pottmann, H. (2011). Geometric Computing for Freeform Architecture. *Journal of Mathematics in Industry*, *1*(1), 1–19. https://doi.org/10.1186/2190-5983-1-4

List of figure captions